Research Article

Fuhua Wei*, Yan Wang, Qinhui Ren, Qin Zhang, Hongliang Chen, and Zhao Liang*

Preparation of Co/Cr-MOFs for efficient removal of fleroxacin and Rhodamine B

https://doi.org/10.1515/gps-2024-0195
received September 07, 2024; accepted December 15, 2024

Abstract: Cr/Co-MOFs were synthesized via a solvothermal method using chromium acetate and cobalt chloride hexahydrate as metal ions, and trimeric acid as the organic ligand. The structures of Cr/Co-MOFs were characterized using Fourier infrared spectroscopy, X-ray diffraction, and scanning electron microscopy techniques. These Cr/Co-MOFs were used for removing organic contaminants in wastewater treatment. Fleroxacin and Rhodamine B (RhB) were specifically selected as target molecules in this study to evaluate the removal efficiency based on the mass of Co/Cr-MOFs, concentrations of organic contaminants, and adsorption time. Experimental findings indicated that at a Co/Cr-MOFs dosage of 100 mg, with initial concentrations of Fleroxacin (30 ppm) and RhB (20 ppm), removal efficiencies achieved were 95% and 99%, respectively. Within a timeframe of 5 h, Co/Cr-MOFs attained adsorption capacities amounting to 269.6 $mg{\cdot}g^{-1}$ for fleroxacin and 289.5 $mg{\cdot}g^{-1}$ for RhB. The interaction between Co/Cr-MOFs and fleroxacin, as well as RhB, is primarily attributed to factors such as pore size, hydrogen bonding, electrostatic charge, and π–π interactions. Moreover, theoretical analysis corroborated these experimental results by demonstrating conformity between the adsorption process and both second-order kinetic model equations alongside Langmuir isotherm model equations. Collectively, the experimental data combined with theoretical investigations underscore the practical significance associated with employing Co/Cr-MOFs for effective eradication of organic pollutants.

Keywords: metal-organic frameworks, antibiotic, dye, wastewater treatment, organic pollutant

*** Corresponding author: Fuhua Wei,** College of Chemistry and Chemical Engineering, Anshun University, Anshun, 561000, Guizhou, China, e-mail: wfh.1981@163.com
*** Corresponding author: Zhao Liang,** Institute of Micro/Nano Materials and Devices, Ningbo University of Technology, Ningbo, 315211, China, e-mail: walleliang@163.com
Yan Wang, **Qinhui Ren**, **Qin Zhang**, **Hongliang Chen:** College of Chemistry and Chemical Engineering, Anshun University, Anshun, 561000, Guizhou, China

1 Introduction

Water pollution poses a serious threat to human health and has a detrimental impact on the environment [1]. Therefore, controlling and treating water pollution are of paramount importance and urgency. Numerous sources contribute to water pollution, including various substances. Among them, emerging organic pollutants have been found to contaminate water supplies, such as pharmaceuticals, cosmetics, as well as industrial pollutants like dyes and pigments [2,3]. Despite their low concentrations, most emerging organic pollutants exhibit considerable resistance to removal through conventional water purification methods due to their physical and chemical properties such as high water solubility [4]. Dyes are used for various purposes, such as artistic endeavors and preservation efforts, in order to introduce color into materials. They provide long-lasting coloring for fabric and fiber surfaces while displaying resistance against exposure to light and detergents [5–7]. In contrast, pigments used in plastics, fibers, and polymer materials remain insoluble within the medium they are applied to [8]. Consequently, wastewater from dye processing companies is discharged into the environment after the dyeing process, leading to water resource pollution. Research suggests that the release of colored wastewater disrupts oxygen dispersion and self-purification mechanisms within aquatic systems [9–11]. The presence of a visible colored layer forms on the water surface when mixed with a water source due to its lower density compared to water. This layer hinders sunlight penetration through the water surface, impeding photosynthesis and respiration processes of underwater organisms [12,13]. The emergence of another group of pollutants in water has been attributed to the commercialization and usage of antibiotics for treating bacterial infections. Approximately 90% of antibiotic active components enter the environment through excretion via urine and feces [14]. Antibiotic contamination poses a global challenge due to potential health issues associated with excessive exposure, which can lead to antibiotic resistance [15]. Research reports have indicated that urban surface water sources, groundwater reservoirs, drinking water supplies,

and wastewater are all contaminated by antibiotics [16]. Therefore, effective strategies need to be implemented for eliminating antibiotics from natural aquatic environments.

A variety of methods is available for removing pollutants from wastewater, including membrane filtration [17], biological treatment [18], adsorption [19], electrochemical treatment [20], advanced oxidation technology [21], among others. However, traditional approaches such as coagulation and filtration have certain drawbacks such as high maintenance costs and operational inconvenience [22]. In contrast, adsorption-based techniques offer potential advantages in terms of cost-effectiveness, energy efficiency, and solution efficacy for pollutant remediation [23]. Recently developed highly efficient adsorbents address these limitations while also meeting the criteria of environmental sustainability and economic viability. One promising class of materials is metal-organic frameworks (MOFs), which possess a large specific surface area [24] and a tunable pore structure that makes them versatile for applications in storage [25,26], sensing [27], separation processes [28], biomedicine [29], and catalysis [30,31]. Among the reported MOFs used for environmental antibiotic treatment, norfloxacin and doxycycline hydrochloride were effectively removed using Zr-MOFs synthesized with 2,5-dihydroxy terephthalic acid and 2-amino-terephthalic acid, respectively. The adsorption capacities of these MOFs reached 134.5 and 148.7 $mg{\cdot}g^{-1}$ [32,33]. Additionally, a bimetallic MOF material Cu/Co-MOFs was utilized to remove doxycycline hydrochloride with a maximum adsorption capacity of 268.5 $mg{\cdot}g^{-1}$ [34].

Due to the limited removal efficiency of monomer MOFs, precise control over the structure and function of bimetallic MOFs can be achieved by modifying metal nodes and organic ligands to meet diverse application requirements. Moreover, bimetallic MOFs demonstrate a synergistic effect in pollutant removal, thereby enhancing the effectiveness of MOF-based pollutant elimination.

The objective of this study was to create functional materials and utilize them for the degradation of organic pollutants, with a specific focus on fleroxacin and Rhodamine B (RhB). To achieve this, Cr/Co-MOFs was synthesized by combining cobalt chloride hexahydrate and chromium acetate as metal precursors, along with 1,3,5-benzoic acid as the organic linker. Subsequently, these Cr/Co-MOFs were employed for effectively eliminating organic pollutants.

2 Experiment

2.1 Experimental material

In the conducted experiment, ligands such as fleroxacin (98%, obtained from Shanghai Aladdin Biochemical Technology Co., Ltd), RhB (analytical reagent (AR), provided by Shanghai McLean Biochemical Technology Co., Ltd), and 1,3,5-benzoic acid (98%, supplied by Shanghai Meryer Biochemical Technology Co., Ltd) were utilized. Metal sources including chromium acetate (AR, supplied by Shanghai Yien Chemical Technology Co., Ltd) and cobalt chloride hexahydrate (AR, obtained from Shanghai Aladdin Biochemical Technology Co., Ltd) were employed.

2.2 Preparation of Cr/Co-MOFs materials

The experimental procedure is illustrated in Figure 1. A total of 0.3000 g (0.0014 mol) of 1,3,5-benzoic acid, 0.3271 g (0.0014 mol) of chromium acetate, and 0.3397 g (0.0014 mol) of cobalt chloride hexahydrate were precisely weighed and placed in three separate small beakers with a capacity of 50 mL each, along with 10 mL of *N,N*-dimethylformamide (DMF) as the organic solvent. The mixture was completely dissolved using an ultrasonic cleaning machine before being transferred to a reaction kettle and subjected to constant temperature drying at 120°C for a duration of 12 h. After the reaction was complete, the mixture was cooled down to room temperature and filtered to obtain Cr/Co-MOFs product, which underwent three rounds of washing using DMF and distilled water separately. Following filtration, the resulting product was dried at 60°C for an additional period of 12 h in a drying oven to yield Cr/Co-MOFs.

2.3 Removal of fleroxacin and RhB by Cr/Co-MOFs materials

The adsorption performance of Cr/Co-MOF toward organic pollutants was investigated by selecting fleroxacin and RhB as target molecules at room temperature (approximately 15°C) and within a pH range of 6–8. Different quantities (20, 30, 50, 100 mg) of Cr/Co-MOFs were introduced into solutions containing varying concentrations (10, 30, 50 $mg{\cdot}L^{-1}$) of fleroxacin. Similarly, various quantities (30, 50, 100 mg) of Cr/Co-MOFs were added to solutions with different concentrations (20, 30, 50 $mg{\cdot}L^{-1}$) of RhB. The mixtures were gently stirred under ambient light conditions. At regular intervals of every half an hour, samples were collected and the concentrations of both fleroxacin and RhB in the solutions were analyzed using an ultraviolet spectrometer. The calculation formula used for analysis remained unchanged.

$$q_e = \frac{(C_0 - C_e)V}{m} \tag{1}$$

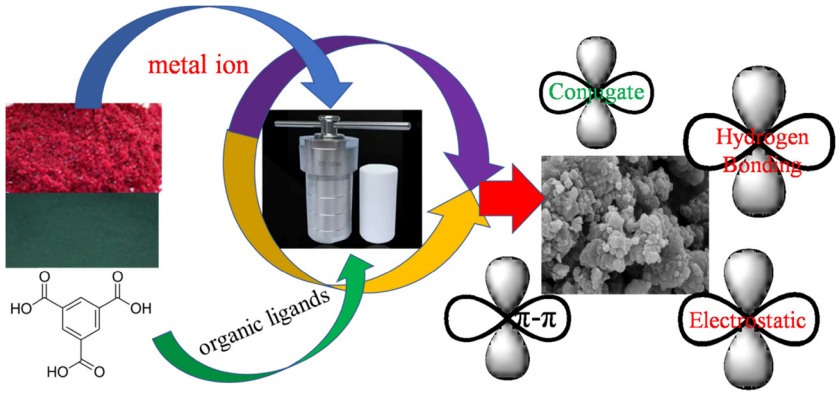

Figure 1: The experimental procedure.

$$\text{Removal rate } (\%) = \frac{(C_0 - C_t)}{C_0} \times 100\% \quad (2)$$

where C_0 denotes the initial concentration of fleroxacin (RhB), C_e represents the concentration at adsorption equilibrium, C_t signifies the concentration at a specific time point t, V indicates the volume of the solution, and m corresponds to the mass of Cr/Co-MOFs.

3 Results and discussion

Based on the Fourier infrared spectroscopy (FT-IR) diagram (Figure 2), we observed two prominent bands at 1,561 and 1,374 cm^{-1}, indicating the equivalent state of the two carboxyl groups after delocalization. These bands are indicative of the reaction between metal ions and carboxyl groups. It is important to note that previous studies have reported that the antisymmetric stretching vibration of carboxyl groups typically occurs within the range of 1,610–1,560 cm^{-1}, while symmetric stretching vibration appears within the range of 1,420–1,300 cm^{-1} [35,36]. The absorption peak at 1,105 cm^{-1} corresponds to C–O bond stretching vibration, whereas the peak at 722 and 765 cm^{-1} suggests substitution on benzene ring. Additionally, when analyzing the X-ray diffraction (XRD) pattern (Figure 3) and scanning electron microscopy (SEM) (Figure 4), we observed a well-defined morphology and structure with excellent dispersion in Co/Cr-MOFs. This high crystallinity can be attributed to weakened or even eliminated intermolecular interactions among organic ligands, which facilitates crystal growth in solvents.

The Thermogravimetry (TG) method is used to investigate the relationship between temperature and mass changes of a substance. As depicted in Figure 5, Co/Cr-MOFs can be divided into two distinct stages within the temperature

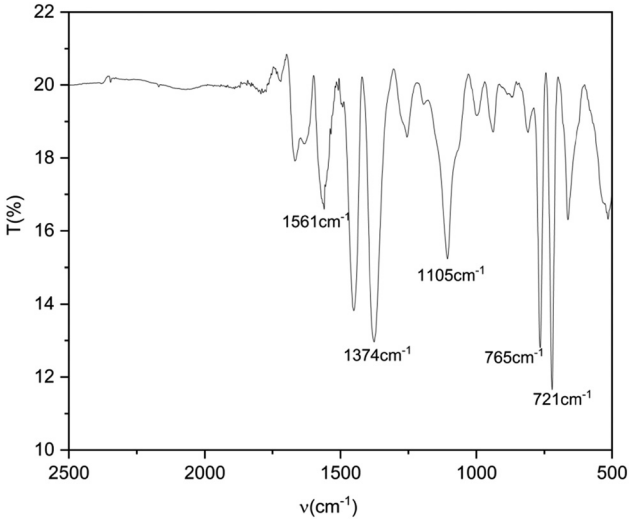

Figure 2: Infrared spectroscopy of Cr/Co-MOFs.

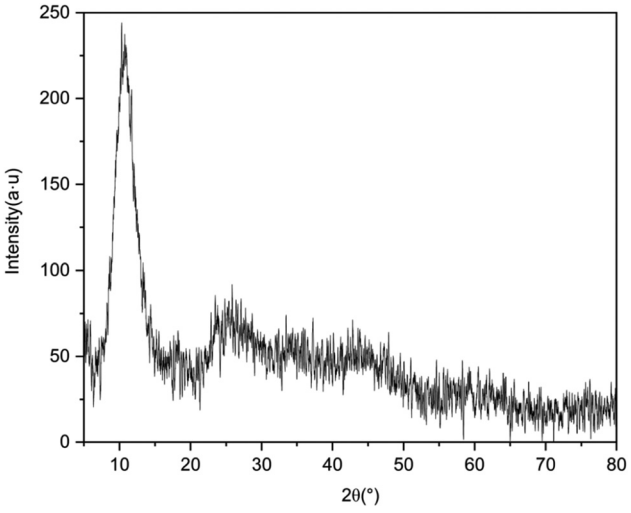

Figure 3: XRD analysis of Cr/Co-MOFs.

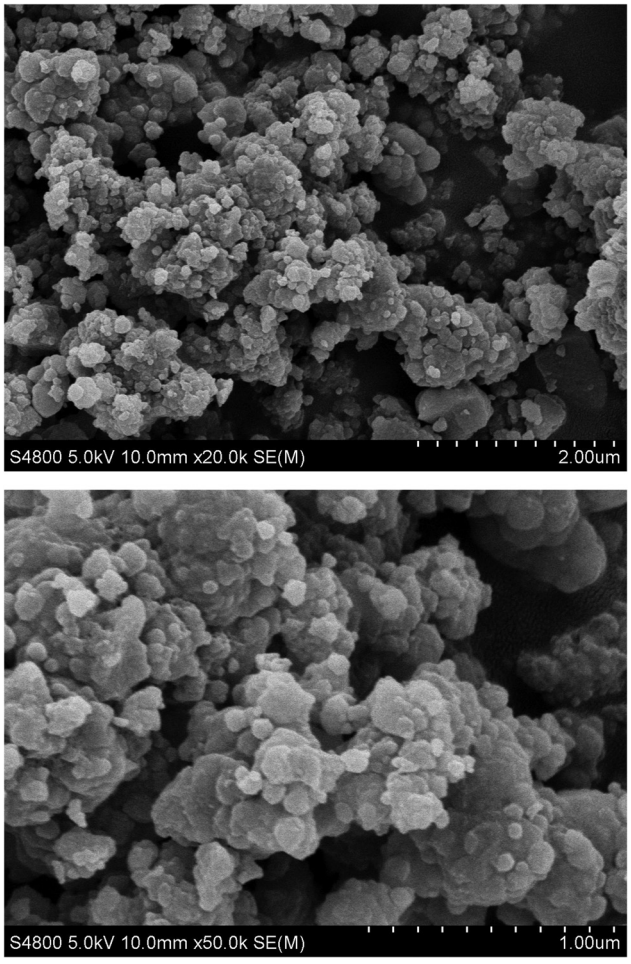

Figure 4: SEM analysis of Cr/Co-MOFs.

range of 800°C. In the initial stage, below 140°C, there is primarily evaporation of solvent molecules from the Co/Cr-MOFs sample, resulting in approximately a 10% reduction in weight. Subsequently, starting at around 350°C and continuing until about 560°C, there is significant collapse of the framework structure with complete degradation of its main constituents while retaining approximately 32% residual content. This figure illustrates that Co/Cr-MOFs exhibit exceptional stability prior to reaching temperatures above 350°C without any noticeable structural deterioration.

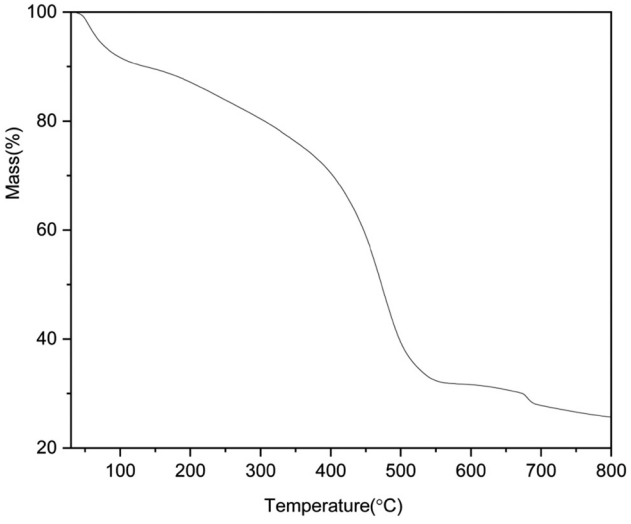

Figure 5: Thermogravimetric analysis of Cr/Co-MOFs.

3.1 Adsorption of fleroxacin and RhB by Co/Cr-MOFs

In this study, the adsorption properties of Co/Cr-MOFs on organic pollutants were investigated with fleroxacin and RhB as individual target molecules. The experimental parameters, including the quantity of Co/Cr-MOFs, the

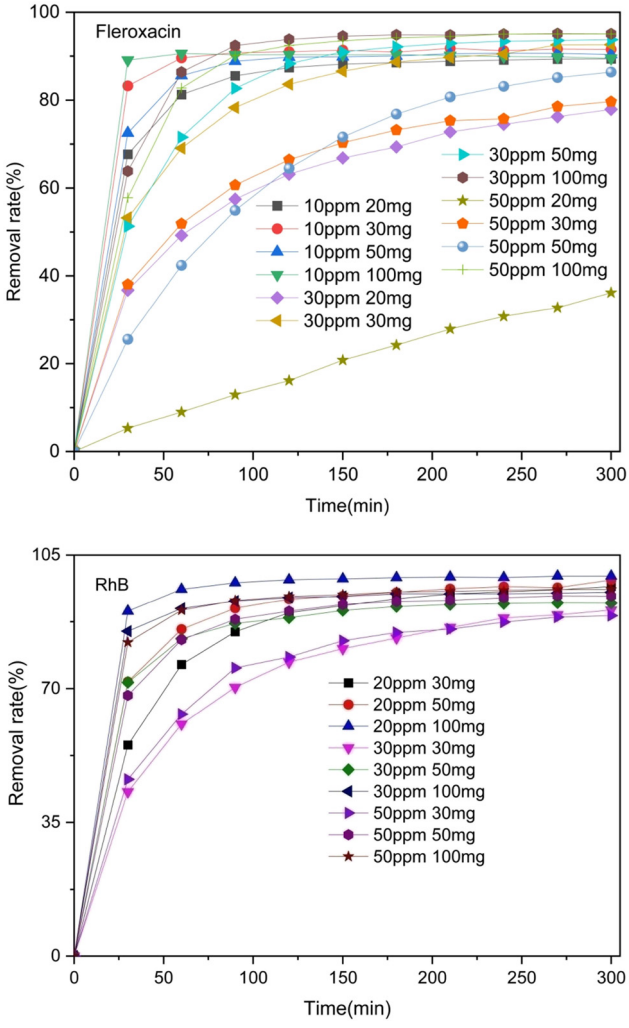

Figure 6: Reactivity of Co/Cr-MOFs toward the removal of organic pollutants.

concentration of organic pollutants, and the reaction duration, were systematically investigated. As shown in Figure 6, a removal rate of 95% was achieved for fleroxacin when using 100 mg of Co/Cr-MOFs with a concentration of 30 ppm. Similarly, a removal rate of 99% was obtained for RhB when using 100 mg of Co/Cr-MOFs with a concentration of 20 ppm. Furthermore, our experimental results indicate that increasing the amount of Co/Cr-MOFs resulted in higher removal rates for both compounds under constant concentrations. Conversely, keeping the amount constant while decreasing the concentrations led to an increasing trend in removal rate due to enhanced exposure and participation at active sites during adsorption processes. Additionally, decreased concentrations weakened competitive adsorption and allowed more molecules to be adsorbed at each active site.

3.2 Adsorption kinetics of fleroxacin and RhB by Co/Cr-MOFs

To further elucidate the mechanism underlying the elimination of fleroxacin and RhB by Co/Cr-MOFs, we employed two simulation models to gain a better understanding of the process. These models are based on different assumptions and formulas that accurately depict the changes in concentrations of fleroxacin and RhB during adsorption. The kinetic equation is presented as follows:

$$\ln C_t/C_0 = k_1 t \tag{3}$$

$$\frac{t}{q_t} = \frac{t}{q_e} + \frac{1}{k_2 q_e^2} \tag{4}$$

$$q_t = k_3 t^{1/2} \tag{5}$$

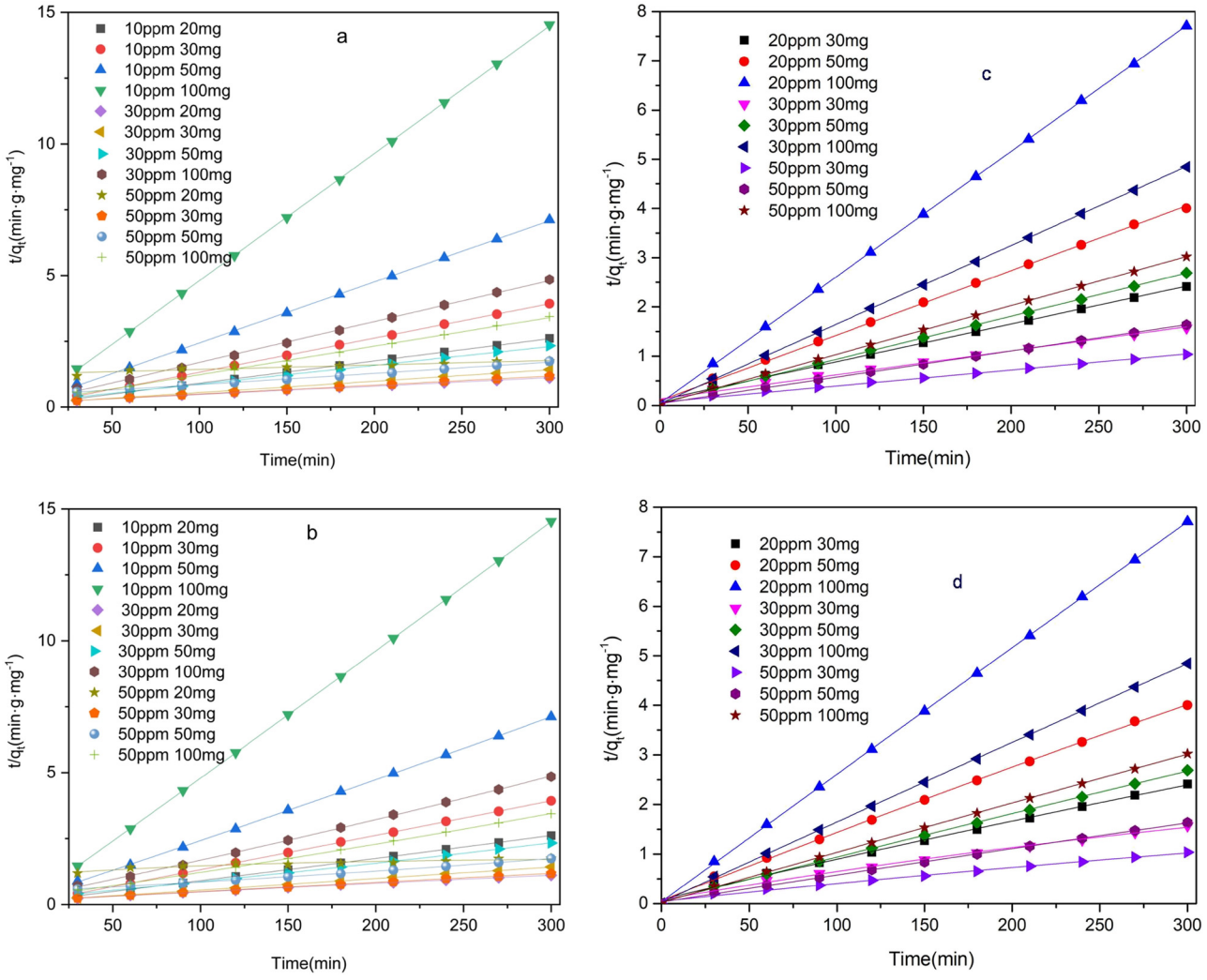

Figure 7: Pseudo-second-order kinetic model for the removal of organic pollutants using Co/Cr-MOFs: (a and b) fleroxacin; (c and d) RhB; (a and c) linear; (b and d) non-linear.

where the variables C_t, C_0, k_1, and k_2, represent the levels of fleroxacin and RhB at a given time point (t), the initial concentrations of fleroxacin and RhB, the rate constants (expressed in minutes) for kinetic reactions, and the duration of the reaction (also expressed in minutes), respectively. The terms q_t and q_e refer to the concentrations (measured in mg·g^{-1}) of the adsorbent material at a specific time point (t) and when equilibrium is reached.

As shown in Figures 7–9 and Tables 1–5, the second kinetics of fleroxacin and RhB adsorption by Co/Cr-MOFs exhibit higher R^2 values compared to the first kinetics. This indicates a strong agreement between simulation and experiment. It suggests that the adsorption kinetics of fleroxacin and RhB by Co/Cr-MOFs adhere to both linear and nonlinear aspects of the second kinetic model.

3.3 Investigation of the isothermal adsorption kinetics of fleroxacin and RhB using Co/Cr-MOFs

The Langmuir and Freundlich isotherm models were employed to analyze the experimental results. As shown in Figure 10 and Table 6, when 100 mg of Co/Cr-MOFs was added to fleroxacin at a concentration of 50 ppm, the analysis based on the Langmuir and Freundlich models yielded parameters presented in Table 5, resulting in R^2 values of 0.9749 and 0.3236, respectively. Similarly, for RhB at a concentration of 50 ppm with an addition of 30 mg Co/Cr-MOFs, both models provided parameters displayed in the table along with corresponding R^2 values of 0.9763 and 0.9874, respectively. These results indicate that Co/Cr-MOFs exhibit a preference for adhering to the Langmuir model when removing both fleroxacin and RhB.

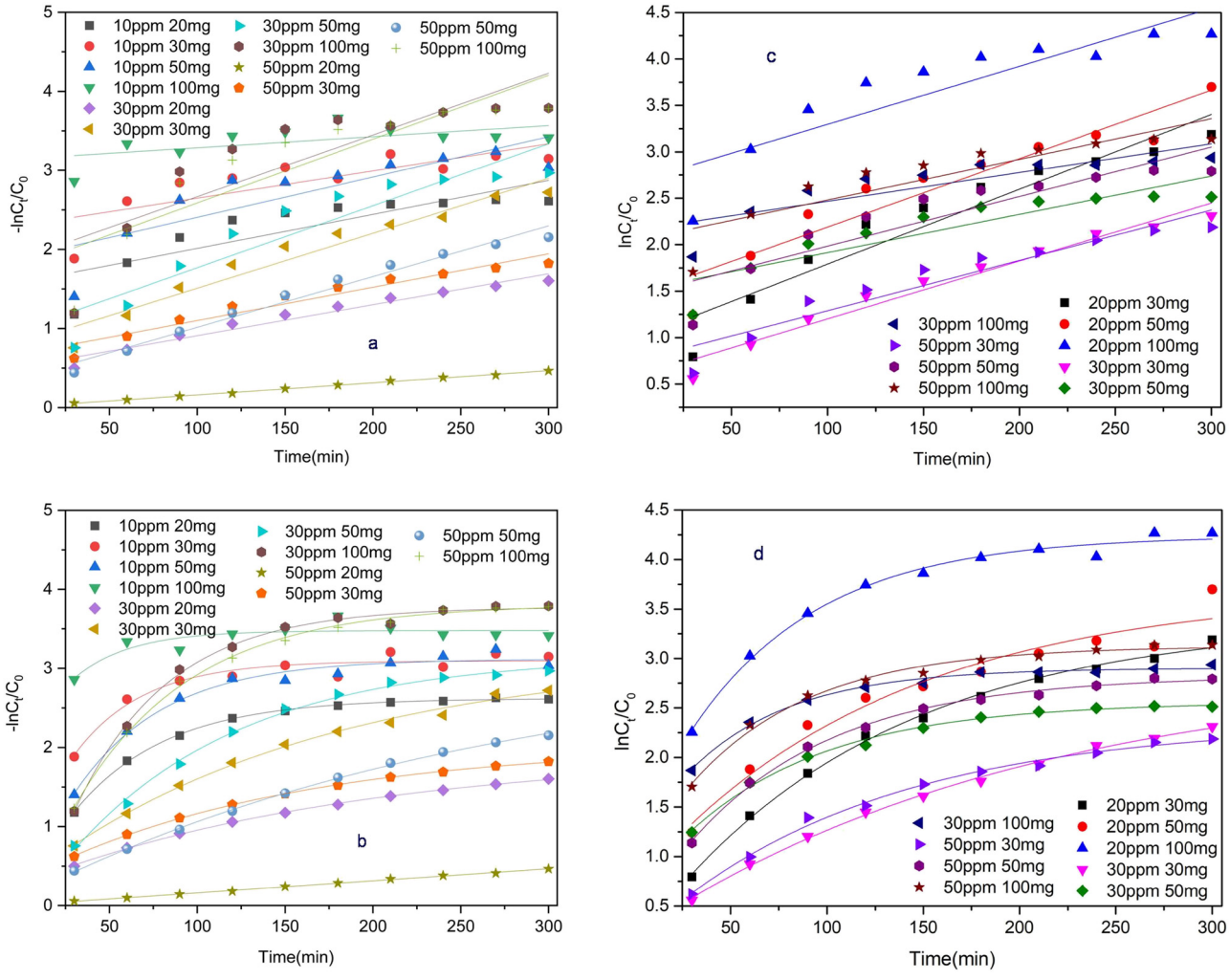

Figure 8: Pseudo-first-order kinetic model for the removal of organic pollutants using Co/Cr-MOFs: (a and b) fleroxacin; (c and d) RhB; (a and c) linear; (b and d) non-linear.

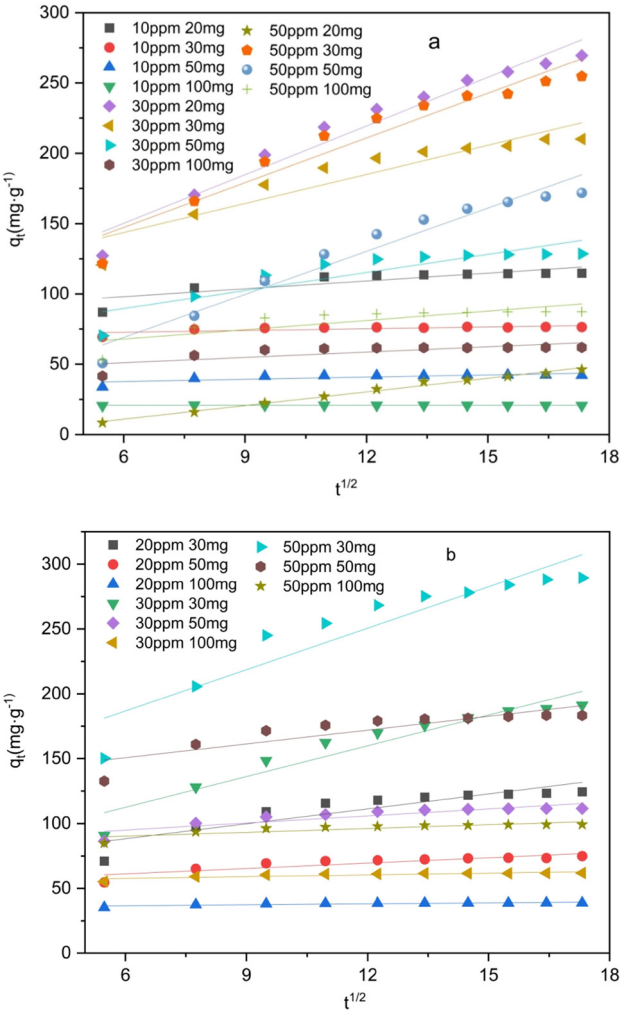

Figure 9: The intraparticle diffusion (IPD) kinetics model for the removal of organic pollutants using Co/Cr-MOFs: (a) fleroxacin; (b) RhB.

3.4 Influence of pH on the adsorption behavior of fleroxacin and RhB onto Co/Cr-MOFs

The pH variations do not affect the adsorption of fleroxacin by Co/Cr-MOFs, as shown in Figure 11. However, the adsorption of RhB gradually decreases with increasing pH levels. This can be mainly attributed to structural changes in both fleroxacin and Rh.

3.5 Influence of temperature on the adsorption behavior of fleroxacin and RhB onto Co/Cr-MOFs

The adsorption capacity of Co/Cr-MOFs for fleroxacin and RhB gradually decreases as the temperature increases. This can be attributed to the increased molecular movement at higher temperatures, which leads to a greater chance of collisions with Co/Cr-MOFs and subsequent escape of more molecules, resulting in reduced adsorption. Additionally, elevated temperatures increase the internal energy of molecules, making it easier for them to detach from the surface of Co/Cr-MOFs and consequently reducing their adsorption capacity. To further investigate the influence of temperature, 100 mg of Co/Cr-MOFs were introduced into solutions with varying temperatures containing fleroxacin at a concentration of 50 ppm; similarly, 30 mg of Co/Cr-MOFs were added to solutions with different temperatures containing RhB at a concentration of 50 ppm. These experimental conditions were compared against

Table 1: Kinetic parameters for the adsorption of RhB over the Co/Cr-MOFs (linear)

Concentration (ppm) (±5%)	Mass (mg) (±1%)	Pseudo-second-order (PSO) model		Pseudo-first-order (PFO) model		$q_{max,exp}$ (mg·g^{-1})
		K_2 (g·mg^{-1}·min^{-1})	R^2	K_1 (L·min^{-1})	R^2	
20	30	0.02076	0.9960	0.43836	0.9062	124.5
	50	0.01714	0.9988	0.4425	0.8891	74.9
	100	0.00406	0.9999	0.75364	0.7673	38.9
30	30	0.02564	0.9880	0.10306	0.9611	191.2
	50	0.00464	0.9993	0.30631	0.7798	111.6
	100	0.00235	0.9999	0.27228	0.6899	61.9
50	30	0.007	0.9926	0.21495	0.8990	289.5
	50	0.00255	0.9989	0.46649	0.7971	183.3
	100	0.00173	0.9998	0.40744	0.7505	99.3

Table 2: Kinetic parameters for the adsorption of fleroxacin over the Co/Cr-MOFs (linear)

Concentration (ppm) (±5%)	Mass (mg) (±1%)	PSO model		PFO model		$q_{max,exp}$ (mg·g^{-1})
		K_2 (g·mg^{-1}·min^{-1})	R^2	K_1(L·min^{-1})	R^2	
10	20	0.0084	0.9997	0.0043	0.6725	124.5
	30	0.0129	0.9999	0.0034	0.5910	74.9
	50	0.0232	0.9997	0.0051	0.6610	42.3
	100	0.0483	0.9999	0.0014	0.2774	38.9
30	20	0.0032	0.9989	0.0039	0.9570	191.2
	30	0.0043	0.9997	0.0069	0.9415	210.1
	50	0.0071	0.9980	0.0078	0.8481	111.6
	100	0.0155	0.9986	0.1178	0.6811	61.9
50	20	0.0016	0.8495	0.0015	0.9976	289.5
	30	0.0034	0.9995	0.0042	0.9328	183.3
	50	0.0042	0.9966	0.0064	0.9763	171.8
	100	0.0108	0.9982	0.0080	0.7590	99.3

Table 3: Kinetic parameters for the adsorption of fleroxacin over the Co/Cr-MOFs (nonlinear)

Concentration (ppm) (±5%)	Mass (mg) (±1%)	PSO model		PFO model	
		K_2 (g·mg^{-1}·min^{-1})	R^2	K_1 (L·min^{-1})	R^2
10	20		0.9999		0.9989
	30		0.9999		0.9323
	50		0.9999		0.9754
	100		0.9999		0.7475
30	20		0.9997		0.9990
	30		0.9997		0.9939
	50		0.9998		0.9957
	100		0.9995		0.9954
50	20		0.8909		0.9973
	30		0.9995		0.9995
	50		0.9998		0.9989
	100		0.9993		0.9972

normal temperature conditions. The enthalpy change and entropy change were determined using the van't Hoff equation as follows:

$$\ln K_0 = \frac{\Delta S^0}{R} - \frac{\Delta H^0}{RT} \quad (6)$$

$$\Delta G^0 = -RT \ln K_0 \quad (7)$$

Table 4: Kinetic parameters for the adsorption of RhB over the Co/Cr-MOFs (nonlinear)

Concentration (ppm) (±5%)	Mass (mg) (±1%)	PSO model		PFO model	
		K_2 (g·mg^{-1}·min)$^{-1}$)	R^2	K_1 (L·min^{-1})	R^2
20	30		0.9962		0.9963
	50		0.9991		0.9490
	100		0.9999		0.9886
30	30		0.9921		0.9972
	50		0.9993		0.9941
	100		0.9999		0.9916
50	30		0.9939		0.9934
	50		0.9990		0.9964
	100		0.9998		0.99012

Table 5: IPD kinetic parameters for the adsorption of RhB and fleroxacin over the Co/Cr-MOFs

Fleroxacin				RhB			
Concentration (ppm) (±5%)	**Mass (mg) (±1%)**	**K_3 (g·mg^{-1}·min$^{-0.5}$)**	**R^2**	**Concentration (ppm) (±5%)**	**Mass (mg) (±1%)**	**K_3 (g·mg^{-1}·min$^{-0.5}$)**	**R^2**
10	20	1.85421	0.65133	20	30	3.83061	0.77507
	30	0.41626	0.51984		50	1.38296	0.76014
	50	0.51866	0.54236		100	0.23834	0.66434
	100	0.0008621	0.12387	30	30	7.90029	0.90911
30	20	11.52947	0.95393		50	1.80934	0.76137
	30	6.88934	0.85795		100	0.44795	0.70141
	50	4.29133	0.75248	50	30	10.65078	0.85003
	100	1.25441	0.53433		50	3.54438	0.73096
50	20	3.22826	0.98994		100	0.97485	0.70014
	30	10.58875	0.92429				
	50	10.22471	0.9506				
	100	2.20339	0.59957				

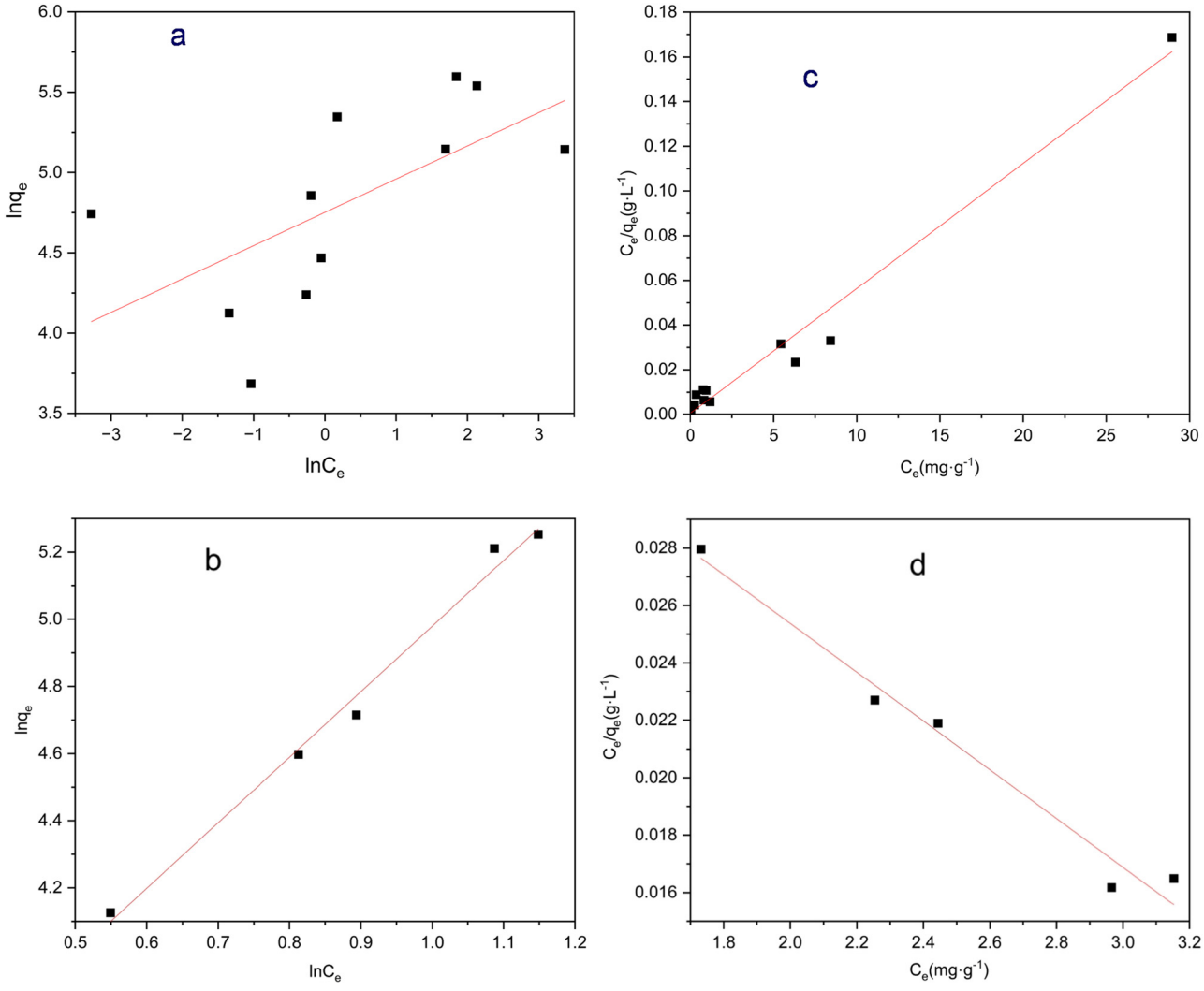

Figure 10: Isothermal modeling of organic pollutant removal by Co/Cr-MOFs: (a and c) fleroxacin; (b and d) RhB; (a and b) Freundlich isotherm; (c and d) Langmuir isotherm.

Table 6: Summary of Langmuir and Freundlich isotherm constants pollution by Co/Cr-MOFs

Adsorbent	Langmuir isotherm		Freundlich isotherm	
	K	R^2	$1/n$	R^2
Fleroxacin	5.59×10^{-6}	0.9749	0.2072	0.3236
RhB	−0.0085	0.9763	1.9528	0.9874

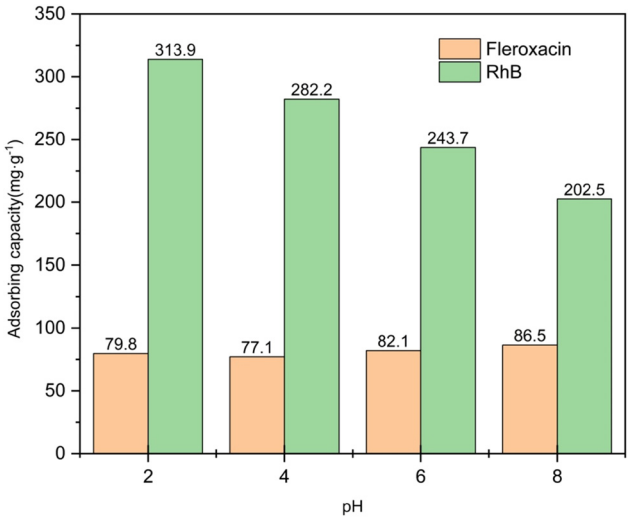

Figure 11: Influence of pH on the adsorption behavior of organic pollutants by Co/Cr-MOFs.

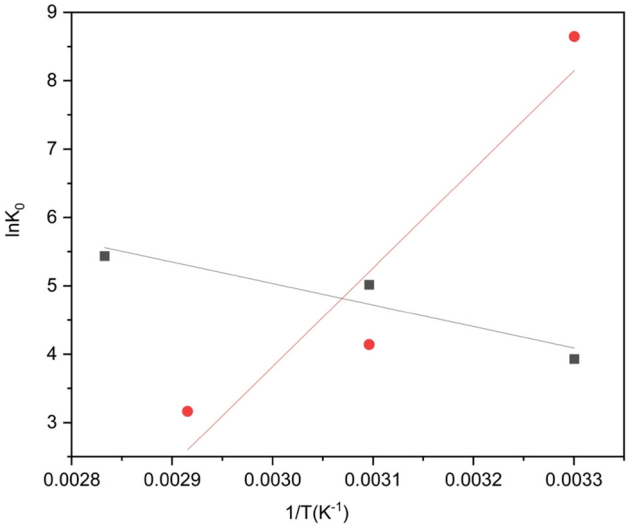

Figure 12: Influence of temperature on the adsorption behavior of organic pollutants by Co/Cr-MOFs.

$$K_0 = \frac{q_e}{c_e} \tag{8}$$

Table 7: Van't Hoff parameters of organic pollution adsorption onto Co/Cr-MOFs (20°C)

Pollutant	$\Delta G°$ (kJ·mol^{-1})	$\Delta H°$ (−slope × R) (kJ·mol^{-1})	$S°$ (intercept × R) (J·mol^{-1}·K^{-1})
Fleroxacin	−9.15	26.1	120.3
RhB	−23.8	−119.8	−327.7

Table 8: Comparative analysis of RhB adsorption using various adsorbents

Adsorbent	q_{max}	pH	Ref.
Azolla pinnata	199.7	3.6	[39]
Zeolitic imidazolate frameworks	85	10<	[40]
Casuarina equisetifolia cone powder	49.5	2	[41]
Bi_2O_3-bentonite nanocomposite	69	3	[42]
Dowex 5WX8 resin	43.4	2.8	[43]
Aleurites Moluccana waste seeds	117	6	[44]
Activated sugar-based carbon	123.4	2–11	[45]
Casuarina equisetifolia needles	82.3	4.4	[46]
Co/Cr-MOFs	313.9	2	This work

The experimental results presented in Figure 12 and Table 7 reveal that the adsorption behavior of RhB on Co/Cr-MOFs is characterized by an exothermic nature and a non-spontaneous process. On the other hand, the adsorption of fleroxacin on Co/Cr-MOFs is found to be exothermic and spontaneous. The mechanism underlying this adsorption process involves a combination of physical and chemical processes, with an enthalpy change exceeding 84 kJ·mol^{-1} primarily attributed to chemisorption. Physical adsorption is indicated for enthalpy changes below 84 kJ·mol^{-1} [37,38]. Hence, it can be inferred that fleroxacin predominantly undergoes chemisorptive adsorption on Co/Cr-MOFs while RhB mainly experiences physical adsorption.

In brief, the adsorption capacity of Co/Cr-MOFs on organic pollutants was assessed by employing a kinetic model that incorporates the isothermal equation and van't Hoff equation, in conjunction with Table 8. The adsorption characteristics of Co/Cr-MOFs toward fleroxacin and RhB can be described as follows: First, based on our observations from adsorption and desorption experiments under an N_2 atmosphere, it is evident that Co/Cr-MOFs possess a significant specific surface area and pore size that enable simultaneous adsorption of both fleroxacin and RhB. Additionally, hydrogen bonding may also play a role in the interaction between Co/Cr-MOFs and these compounds. Furthermore, pH-dependent studies have revealed potential free groups on the surface of Co/Cr-MOFs that facilitate electrostatic interactions

with both compounds. Moreover, taking into account the presence of benzene rings in both fleroxacin and RhB as well as aromatic rings in Co/Cr-MOFs; π–π bond formation could further enhance their affinity for each other. As a result, all these factors collectively contribute to the exceptional adsorption performance demonstrated by Co/Cr-MOFs toward fleroxacin and RhB [47–50].

4 Conclusion

The Co/Cr-MOFs material was successfully synthesized using the solvothermal method, and its morphology and structure were characterized through XRD, SEM, FTIR, and TG techniques. Afterwards, we utilized the as-characterized Co/Cr-MOFs material to efficiently remove fleroxacin and RhB. Through systematic variations in the mass of Co/Cr-MOFs material, concentration of fleroxacin and RhB in solution, as well as pH conditions during adsorption experiments, the experimental findings clearly demonstrate that Co/Cr-MOFs exhibit impressive adsorption capacities toward fleroxacin (269.6 $mg{\cdot}g^{-1}$) and RhB (313.9 $mg{\cdot}g^{-1}$) within a 5-h timeframe. The Co/Cr-MOFs exhibited removal efficiencies of 95.1% and 99.5% for fleroxacin and RhB, within a duration of 5 h, respectively. Moreover, the analysis of kinetic modeling reveals excellent agreement with the pseudo-second order kinetics model for the adsorption of both target pollutants onto Co/Cr-MOFs. Additionally, the Langmuir and Freundlich isotherm analyses indicate multi-layer adsorption for fleroxacin, while single-layer adsorption occurs for RhB on the surface of Co/Cr-MOFs materials. These collective results strongly emphasize the promising potential of utilizing Co/Cr-MOFs materials for effectively removing fleroxacin and RhB contaminants in practical applications.

Acknowledgements: This work was supported by Doctoral Fund of Anshun University (asxybsjj202103), Key Laboratory of Agricultural Resources and Environment in High Education Institute of Guizhou Province (Qianjiaoji[2023]25).

Funding information: Doctoral Fund of Anshun University (asxybsjj202103).

Author contributions: Fuhua Wei: writing – original draft and writing – review and editing; Yan Wang and Qin Zhang: methodology and investigation; Qinhui Ren: formal analysis and methodology; Hongliang Chen: conceptualization; Zhao Liang: validation and software.

Conflict of interest: Authors state no conflict of interest.

Data availability statement: The datasets generated during and/or analyzed during the current study are available from the corresponding author on reasonable request.

References

[1] Pouramini Z. The VOCs catalytic combustion by perovskite catalysts: A mini-review. Adv Appl NanoBio-Technol. 2022;3:23–30.
[2] Liang W, Wang B, Cheng J, Xiao D, Xie Z, Zhao J. 3D, eco-friendly metal-organic frameworks@ carbon nanotube aerogels composite materials for removal of pesticides in water. J Hazard Mater. 2021;401:123718.
[3] Naskar J, Boatemaa MA, Rumjit NP, Thomas G, George P, Lai CW, et al. Recent advances of nanotechnology in mitigating emerging pollutants in water and wastewater: status, challenges, and opportunities. Water Air Soil Pollut. 2022;233:156.
[4] Wei F, Wang K, Li W, Ren Q, Qin L, Yu M, et al. Preparation of Fe/Ni-MOFs for the adsorption of ciprofloxacin from wastewater. Molecules. 2023;28:4411.
[5] Pouramini Z, Ayati B, Babapoor A. Enhancing PFC ability to dye removal and power generation simultaneously via conductive spheres in the anodic chamber. J Electroanal Chem. 2022;917:116410.
[6] Deb A, Das S, Debnath A. Fabrication and characterization of organometallic nanocomposite for efficient abatement of dye laden wastewater: CCD optimization, adsorption mechanism, co-existing ions, and cost analysis. Chem Phys Lett. 2023;830:140820.
[7] Brazesh B, Mousavi SM, Zarei M, Ghaedi M, Bahrani S, Hashemi SA. Biosorption. In Interface science and technology. Vol. 33. Amsterdam, The Netherlands: Elsevier; 2021. p. 587–628.
[8] Hashemi SA, Mousavi SM, Ramakrishna S. Effective removal of mercury, arsenic and lead from aqueous media using Polyaniline-Fe_3O_4-silver diethyldithiocarbamate nanostructures. J Clean Prod. 2019;239:118023.
[9] Wei F, Gong J, Ren Q, Yu X, Wang Y, Chen H, et al. Reparation of Zn/Zr-MOFs by microwave-assisted ball milling and adsorption of lomefloxacin hydrochloride and levofloxacin hydrochloride in wastewater. Environ Res. 2024;252:118941.
[10] Saravanan S, Kumar PS, Chitra B, Rangasamy G. Biodegradation of textile dye Rhodamine-B by Brevundimonas diminuta and screening of their breakdown metabolites. Chemosphere. 2022;308:136266.
[11] Das S, Pal A, Debnath A. Polyaniline-coated magnesium ferrite nanocomposite: synthesis, characterization, fabrication cost analysis and dye sorption behavior with scale-up design. ChemistrySelect. 2023;8:e202300928.
[12] Amini ZP, Babapoor A. Using nanomembrane to heavy metal removal from wastewater: A mini-review. Adv Appl NanoBio-Technol. 2022;3:7–13.
[13] Uddin MJ, Ampiaw RE, Lee W. Adsorptive removal of dyes from wastewater using a metal-organic framework: A review. Chemosphere. 2021;284:131314.
[14] Hashemi SA, Bahrani S, Mousavi SM, Mojoudi F, Omidifar N, Lankarani KB, et al. Development of sulfurized Polythiophene-Silver Iodide-Diethyldithiocarbamate nanoflakes toward Record-High

and selective absorption and detection of mercury derivatives in aquatic substrates. Chem Eng J. 2022;440:135896.
[15] Buonomenna MG, Mousavi SM, Hashemi SA, Lai CW. Water cleaning adsorptive membranes for efficient removal of heavy metals and metalloids. Water. 2022;14:2718.
[16] Jurado A, Walther M, Díaz-Cruz MS. Occurrence, fate and environmental risk assessment of the organic microcontaminants included in the Watch Lists set by EU Decisions 2015/495 and 2018/840 in the groundwater of Spain. Sci Total Environ. 2019;663:285–96.
[17] Aghajani M, Torabi SA, Heydari JJS-EPS. A novel option contract integrated with supplier selection and inventory prepositioning for humanitarian relief supply chains. Socio-Econ Plan Sci. 2020;71:100780.
[18] Wei F, Ren Q, Wang N, Chen H, Zhang Y, Liang Z. Efficient removal of norfloxacin from water by Fe-MOFs. Quim Nova. 2024;47(9):e-20240073.
[19] Stylianou M, Christou A, Michael C, Agapiou A, Papanastasiou P, Fatta-Kassinos D. Adsorption and removal of seven antibiotic compounds present in water with the use of biochar derived from the pyrolysis of organic waste feedstocks. J Environ Chem Eng. 2021;9:105868.
[20] Wei F, Zhang Q, Ren Q, Chen H, Zhang Y, Liang Z. Zn/Cr-MOFs/TiO_2 composites as adsorbents for levofloxacin hydrochloride removal. Molecules. 2024;29(18):4477.
[21] Masood Z, Ikhlaq A, Akram A, Qazi UY, Rizvi OS, Javaid R, et al. Application of nanocatalysts in advanced oxidation processes for wastewater purification: Challenges and future prospects. Catalysts. 2022;12:741.
[22] Azhdari R, Mousavi SM, Hashemi SA, Bahrani S, Ramakrishna S. Decorated graphene with aluminum fumarate metal organic framework as a superior non-toxic agent for efficient removal of Congo Red dye from wastewater. J Environ Chem Eng. 2019;7:103437.
[23] Zhang J, Si M, Jiang L, Yuan X, Yu H, Wu Z, et al. Core-shell Ag@nitrogen-doped carbon quantum dots modified $BiVO_4$ nanosheets with enhanced photocatalytic performance under Vis-NIR light: Synergism of molecular oxygen activation and surface plasmon resonance. Chem Eng J. 2021;410:128336.
[24] Li Z, Wang L, Qin L, Lai C, Wang Z, Zhou M, et al. Recent advances in the application of water-stable metal-organic frameworks: Adsorption and photocatalytic reduction of heavy metal in water. Chemosphere. 2021;285:131432.
[25] Peng Y, Xu J, Xu J, Ma J, Bai Y, Cao S, et al. Metal-organic framework (MOF) composites as promising materials for energy storage applications. Adv Colloid Interface Sci. 2022;307:102732.
[26] Hong AN, Yang H, Bu X, Feng P. Pore space partition of metal-organic frameworks for gas storage and separation. Energy Chem. 2022;4:100080.
[27] Ma Y, Zhao Z, Zhu M, Zhang Y, Kosinova M, Fedin VP, et al. Rapid detection of lamotrigine by a water stable fluorescent lanthanide metal–organic framework sensor. Polyhedron. 2022;220:115803.
[28] Geng C, Sun Y, Zhang Z, Qiao Z, Zhong C. Mitigated aging in a defective metal-organic framework pillared polymer of an intrinsic porosity hybrid membrane for efficient gas separation. ACS Sustain Chem Eng. 2022;10:3643–50.
[29] Asadniaye Fardjahromi M, Nazari H, Ahmadi Tafti SM, Razmjou A, Mukhopadhyay S, Warkiani ME. Metal-organic framework-based nanomaterials for bone tissue engineering and wound healing. Mater Today Chem. 2022;23:100670.
[30] Rostamnia S, Xin H, Nouruzi N. Metal–organic frameworks as a very suitable reaction inductor for selective solvent-free multicomponent reaction: IRMOF-3 as a heterogeneous nanocatalyst for Kabachnik-Fields three-component reaction. Microporous Mesoporous Mater. 2013;179:99–103.
[31] Du C, Zhang Z, Yu G, Wu H, Chen H, Zhou L, et al. A review of metal organic framework (MOFs)-based materials for antibiotics removal via adsorption and photocatalysis. Chemosphere. 2021;272:129501.
[32] Ren Q, Ma Y, Wei F, Qin L, Chen H, Liang Z, et al. Preparation of Zr-MOFs for the adsorption of doxycycline hydrochloride from wastewater. Green Process Synth. 2023;12:20228127.
[33] Wei FH, Liu HY, Ren QH, Yang L, Qin L, Chen HL, et al. Preparation of Zr-MOF for the removal of norfloxacin from an aqueous solution. Inorg Chem Commun. 2023;153:110819.
[34] Wei FH, Nie M, Ren QH, Yu X, Li H, Chen HL, et al. Preparation of bimetallic metal–organic frameworks for adsorbing doxycycline hydrochloride from wastewater. Appl Organomet Chem. 2023;37(8):e7212.
[35] Ezugwu CI, Asraf MA, Li X, Liu SW, Kao CM, Zhuiykov SF, et al. Selective and adsorptive removal of anionic dyes and CO2 with azolium-based metal-organic frameworks. J Colloid Interface Sci. 2018;519:214–23.
[36] Wei F, Yu X, Ren Q, Chen H, Zhang Y, Liang Z. Removal of moxifloxacin from aqueous solutions using GO/Cr-MOFs. J Phys Chem A. 2024;128(37):7889–98.
[37] Hu J, Yu H, Dai W, Yan X, Hu X, Huang H. Enhanced adsorptive removal of hazardous anionic dye Congo red by a Ni/Cu mixed-component metal–organic porous material. RSC Adv. 2014;4:35124.
[38] Wei F, Gong X, Ren Q, Chen H, Zhang Y, Liang Z. Co/Cd-MOF-derived porous carbon materials for moxifloxacin adsorption from aqueous solutions. Molecules. 2024;29(16):3873.
[39] Kooh MRR, Lim LBL, Lim LH, Dahri MK. Separation of toxic rhodamine B from aqueous solution using an efficient low-cost material, *Azolla pinnata*, by adsorption method. Env Monit Assess. 2016;188(2):1–15.
[40] Zhang J, Hu X, Yan X, Feng R, Zhou M, Xue J. Enhanced adsorption of Rhodamine B by magnetic nitrogen-doped porous carbon prepared from bimetallic ZIFs. Colloids Surf A. 2019;575:10–7.
[41] Dahri MK, Kooh MRR, Lim LBL. Remediation of Rhodamine B dye from aqueous solution using *Casuarina equisetifolia* cone powder as a low-cost adsorbent. Adv Phys Chem. 2016;2016:9497378.
[42] Patil SP, Bethi B, Sonawane GH, Shrivastava VS, Sonawane S. Efficient adsorption and photocatalytic degradation of Rhodamine B dye over Bi_2O_3-bentonite nanocomposites: A kinetic study. J Ind Eng Chem. 2016;34:356–63.
[43] Khan MA, Momina, Siddiqui MR, Otero M, Alshareef SA, Rafatullah M. Removal of Rhodamine B from water using a solvent impregnated polymeric Dowex 5WX8 resin: Statistical optimization and batch adsorption studies. Polymers. 2020;12(2):1–12.
[44] Postai DL, Demarchi CA, Zanatta F, Melo DCC, Rodrigues CA. Adsorption of Rhodamine B and methylene blue dyes using waste of seeds of *Aleurites Moluccana*, a low cost adsorbent. Alex Eng J. 2016;55(2):1713–23.
[45] Xiao W, Garba ZN, Sun S, Lawan I, Wang L, Lin M, et al. Preparation and evaluation of an effective activated carbon from white sugar for the adsorption of Rhodamine B dye. J Clean Prod. 2020;253:119989.
[46] Parthasarathy P, Narayanan SK. Determination of kinetic parameters of biomass samples using thermogravimetric analysis. Environ Prog Sustain Energy. 2014;33(1):256–66.

[47] Rego RM, Kurkuri MD, Kigga MA. Comprehensive review on water remediation using UiO-66 MOFs and their derivatives. Chemosphere. 2022;302:134845.
[48] Chen J, Ouyang JB, Chen WQ, Zheng ZP, Yang Z, Liu ZR, et al. Fabrication and adsorption mechanism of chitosan/Zr-MOF (UiO-66) composite foams for efficient removal of ketoprofen from aqueous solution. Chem Eng J. 2022;431:134045.
[49] Ren Q, Wei F, Chen H, Chen D, Ding B. Preparation of Zn-MOFs by microwave-assisted ball milling for removal of tetracycline hydrochloride and Congo red from wastewater. Green Process Synth. 2021;10(1):125–33.
[50] Sriram G, Bendre A, Mariappan E, Altalhi T, Kigga M, Ching YC, et al. Recent trends in the application of metal-organic frameworks (MOFs) for the removal of toxic dyes and their removal mechanism-a review. Sustain Mater Technol. 2022;31:e00378.